

INTERPRETATION OF THE RADIO/X-RAY KNOTS OF AGN JETS WITHIN THE INTERNAL SHOCK MODEL FRAMEWORK

S. SAHAYANATHAN¹ AND R. MISRA²

Draft version November 26, 2018

ABSTRACT

The dynamics of relativistically moving blobs ejected out of a central AGN, are considered. It is assumed that the collision between two blobs are completely inelastic, such that the bulk kinetic energy lost in the collision is used to energize electrons to relativistic energies via acceleration in internal shocks which are formed due to the collision. These high energy electrons which are produced on a time-scale corresponding to the collision time-scale, cool by radiative losses due to synchrotron and Inverse Compton processes. The model is applied to the radio/X-ray knots of several AGN. For three of these sources we have analyzed long (> 40 ksec) *Chandra* observations and report on constrains on the X-ray spectral indices. In the framework of this model the AGN are inferred to sporadically eject relativistic blobs on time-scales ranging from 10^{11} to 10^{12} secs for different sources. It is shown that the collision time-scales can be longer than the age of the knot and, hence, non-thermal electrons are continuously being injected into the system. This continuous injection, in contrast to an instantaneous one time injection, gives rise to a characteristic spectral break, rather than a high-energy cutoff in the spectrum.

Subject headings: Galaxies: active - galaxies: jets - X-rays: galaxies

1. INTRODUCTION

Study of the knots in kilo parsec scale jets of Active Galactic Nuclei (AGN) has been given a new dimension after the advent of *Chandra* which due to its excellent spatial resolution is able to resolve bright X-ray knots of such jets (Chartas *et al.* 2000; Sambruna *et al.* 2002, 2001; Tavecchio *et al.* 2000). In most of the cases, the X-ray knots coincide with their radio/optical counterparts (Sambruna *et al.* 2002; Pesce *et al.* 2001; Sambruna *et al.* 2001; Marshall *et al.* 2001; Wilson & Yang 2002). The discovery of such knots in different energy bands provides useful information about the basic emission mechanism and the underlying acceleration processes involved there. The radio and optical emission from these knots are generally accepted to be of synchrotron origin, whereas the X-ray emission can be due to either synchrotron (Worall *et al.* 2001; Sambruna *et al.* 2002; Pesce *et al.* 2001; Sahayanathan *et al.* 2003) or Inverse Compton processes (Sambruna *et al.* 2001, 2002; Pesce *et al.* 2001; Tavecchio *et al.* 2000; Schwartz *et al.* 2000; Chartas *et al.* 2000; Sahayanathan *et al.* 2003). If the radio-to-optical index (α_{RO}) is larger than the optical-to-X-ray index (α_{OX}), a single emission mechanism cannot explain the observed fluxes (however see Dermer & Atoyan (2002) who show that if Klein-Nishina losses is important, spectral hardening can occur) and the X-ray emission may be due to Inverse Comptonization. On the other hand, if α_{RO} is smaller than α_{OX} , synchrotron origin of X-ray is acceptable (Tavecchio *et al.* 2000; Sambruna *et al.* 2002; Pesce *et al.* 2001). This synchrotron origin of X-rays for knots with $\alpha_{RO} < \alpha_{OX}$, was strengthened for the knots of 3C271 by Pesce *et al.* (2001) who show that the alternate Inverse Compton model would require exceptionally large Doppler factors. When the X-ray emission can be at-

tributed to the Inverse Compton process, the possible choices of target photons are radio/optical synchrotron photons (SSC)(Schwartz *et al.* 2000) or the cosmic microwave background (IC/CMB)(Tavecchio *et al.* 2000; Sambruna *et al.* 2001, 2002; Pesce *et al.* 2001; Sahayanathan *et al.* 2003). Tavecchio *et al.* (2000) have shown that the SSC interpretation would require large jet powers and magnetic fields much lower than the equipartition values whereas IC/CMB requires relatively low jet power and near equipartition magnetic fields.

These possible radiative process identifications have to be associated with (and confirmed by) dynamical models regarding the origin and subsequent evolution of the radiating non-thermal particles. In many models, these non-thermal particles are assumed to be generated by a short duration acceleration process and the particle distribution is determined by radiative losses (Sambruna *et al.* 2001, 2002; Tavecchio *et al.* 2000; Jaffe & Perola 1973; Kardashev 1962; Pacholczyk 1970). The high energy particles cool more efficiently and hence get depleted in time, giving rise to a time-dependent high energy cut off in the non-thermal particle distribution. If the X-ray emission is attributed to synchrotron emission by these particles, then these models predict an exponentially decreasing X-ray spectrum (Sambruna *et al.* 2001, 2002; Tavecchio *et al.* 2000; Pesce *et al.* 2001). On the other hand, it may also be possible that the acceleration process exists for longer than the age of the knot, and hence, there is a continuous injection of non-thermal particles. In this case, a time dependent break in the non-thermal particle distribution occurs at $\gamma = \gamma_c$, where γ_c is determined by the condition that the cooling time-scale for electrons with $\gamma = \gamma_c$ is equal to the age of the knot (Heavens & Meisenheimer 1987; Meisenheimer *et al.* 1989). This model predicts the X-ray spectral index α_X to be $\approx \alpha_R + 1/2$, where α_R is the radio spectral index. Thus the predicted spectrum depends, in particular, on the duration of the non-thermal particle production and, in general, on the production mechanism.

While there is no consensus on the origin of these non-thermal particles, one of the standard models is the internal

¹ Nuclear Research Laboratory, Bhabha Atomic Research Center, Mumbai, India;
sunder@apsara.barc.ernet.in

² Inter-University Center for Astronomy and Astrophysics, Post Bag 4, Ganeshkhind, Pune-411007, India; rmisra@iucaa.ernet.in

shock scenario (Rees 1978; Spada *et al.* 2001), where the particles are energized by Fermi acceleration in shocks produced during the interaction of relativistically moving blobs ejected from the central engines with different speeds. This model has also been used to explain the prompt emission of Gamma-ray Bursts (Rees & Meszaros 1994; Lazzati *et al.* 1999). A detailed description of the shock formation and subsequent electron acceleration is complicated and would require numerically difficult magneto-hydrodynamic simulations. Moreover, the limited number of observables, which can be obtained from the featureless spectra in two or three different energy bands, may not be able to constrain the various assumption and/or the initial conditions of such a detailed study. Nevertheless, a qualitative idea as to whether the internal shock model is consistent with the present observations and if so, qualitative estimates of the model parameters would be desirable. Such an estimate will provide insight into the temporal behavior of the central engine.

In this work, we implement an internal shock model with simplifying assumptions and compute the time-evolution of the non-thermal particles produced. We compare the results obtained with the broad-band fluxes from knots of several AGN jets and their observed positions. The motivation here is to find a consistent set of model parameters that can explain the observations and thereby make qualitative estimates of their values. Apart from the fluxes at different energy bands, the spectral indices in each band can also provide important diagnostic information about the nature of these sources. Hence, we have analyzed long (> 40 ksec) *Chandra* observations of three AGN and report the constrains that were obtained on the X-ray spectral indices of the individual knots.

In the next section, a brief description of the data analysis technique and the results obtained are presented. In §3, the internal shock model and the assumptions used in this work are described while in §4, the results of the analysis are presented and discussed. Throughout this work, $H_0 = 75 \text{ km s}^{-1} \text{ Mpc}^{-1}$ and $q_0 = 0.5$ are adopted.

2. DATA ANALYSIS

Long exposure *Chandra* observations of the sources 1136–135, 1150+497 and 3C371 were performed with the ACIS-S with the source at the aim-point of the S3 chip. The observation ID (Obs. ID) and the exposure time of the observation are tabulated in Table 1. Earlier shorter duration observations of these sources had revealed two bright knots for each source whose positions from the nucleus are tabulated in Table 2. These longer duration observations allow for better constrain on the X-ray spectral indices of these knots.

The reprocessed data from *Chandra* X-ray center were analyzed using the latest calibration files to produce the image and spectra. The X-ray counts from each individual knot was extracted using a circular region centered at the knot. The background was estimated from the counts obtained from same size regions located at the same distance from the nucleus but at different azimuth angles. The radius of the circular region was chosen to be $0.74''$ for the sources 1136–135 and 1150+497, while for 3C371 a smaller radius of $0.6''$ was used. These sizes were chosen to minimize any possible contamination from the nucleus and/or the other knot.

Spectral fits were undertaken on the data using the XSPEC package in C statistic mode which is the appropriate statistic when the total counts are low. The flux and the energy spectral indices obtained are tabulated in Table 1.

TABLE 1
Chandra OBSERVATIONS

Source name	Obs Id	Exposure	Knots	$F_{0.3-3.0}$	α_X
1136–135	3973	77.37	A	0.63	$1.24^{+1.51}_{-0.66}$
			B	1.56	$0.65^{+0.69}_{-0.28}$
1150+497	3974	68.50	A	3.15	$0.66^{+0.28}_{-0.26}$
			B	0.61	$0.90^{+2.22}_{-1.02}$
3C371	2959	40.86	A	3.32	$1.43^{+0.85}_{-0.76}$
			B	7.84	$1.07^{+0.26}_{-0.23}$

NOTE. — Columns:- 1: Source name. 2: *Chandra* Observation Id 3: Exposure time (in ksec) 4: Knots prominent in X-ray 5: Flux in 0.3–3.0 keV energy band in $\text{ergs}/\text{cm}^2/\text{s}$. 6: X-ray energy spectral index.

TABLE 2
OBSERVED KNOT FEATURES

Source name	Type	z	Knot	Position	α_{RO}	α_{OX}	Ref
1136–135	FSRQ	0.554	A	4.5	0.73	0.83	1
			B	6.7	1.04	0.68	
1150+497	FSRQ	0.334	A	2.1	0.99	0.83	1
			B	4.3	1.24	0.44	
1354+195	FSRQ	0.720	A	1.7	1.05	0.6	1
			B	3.6	1.15	0.68	
3C273	QSO	0.158	A	13	0.86	0.61	2
			B	15	0.9	0.73	
3C371	Bl Lac	0.051	A	1.7	0.9	1.28	3
			B	3.1	0.76	1.14	

NOTE. — Columns:- 1: Source name. 2: Type of the source. 3: Redshift. 4: Knots prominent in X-ray. The nomenclature is same for all the knots as they are in the literature except for 3C371 where A and B are reverse. 5: Position of the knot in arc seconds. 6: Radio-to-Optical index. 7: Optical-to-X-ray index. 8: References: 1: Sambruna *et al.* (2002), 2: Sambruna *et al.* (2001), 3: Pesce *et al.* (2001)

3. THE INTERNAL SHOCK MODEL

In the internal shock model framework, temporal variations of the ejection process produces density fluctuations (moving with different velocities) which collide at some distance from the source to produce an observable knot. This distance will depend on the time-scale over which the variation takes place. In general the system will exhibit variations over a wide range of time-scales and knots like features would be produced at different distance scales. In this work, we consider large scale jets (with deprojected distances ≈ 100 kpc) which are expected to arise from variability occurring on a corresponding large time-scale. Variations on smaller time-scales would produce knot structures on smaller distance scales, for example par-sec scale jets or even smaller, which will be unresolved for these sources. These smaller time-scale variabilities will be smoothed out at large distances and hence one expects that the jet structure of these sources to be determined by variations over a single characteristic time-scale. To further simplify the model, we approximate the density and velocity fluctuations as two discrete blobs with equal masses, $M_1 = M_2 = M$, having Lorentz factors, Γ_1 and Γ_2 , that are

ejected one after the other, from the central engine with a time delay of Δt_{12} . The collision of the blobs is considered to be completely inelastic i.e. the blobs coalesce and move as a single cloud, which is identified with the observed knot. From conservation of momentum, the Lorentz factor of the knot is

$$\Gamma = \sqrt{\left(\frac{\Gamma_1\beta_1 + \Gamma_2\beta_2}{2}\right)^2 + 1} \quad (1)$$

where $\beta_{1,2} = v_{1,2}/c$, are the velocities of the blobs normalized to the speed of light. Since the collision is inelastic a fraction of the bulk kinetic energy is dissipated. Denoting all quantities in the rest frame of the knot by subscript K , this energy ΔE_K can be estimated to be,

$$\Delta E_K = [\Gamma_{1K} + \Gamma_{2K} - 2]Mc^2 \quad (2)$$

The Lorentz factors of the blobs in the knot's rest frame $\Gamma_{1K,2K} = (1 - \beta_{1K,2K}^2)^{-1/2}$ are computed using

$$\beta_{1K,2K} = \frac{\beta_{1,2} - \beta}{1 - \beta_{1,2}\beta} \quad (3)$$

where $\beta = \sqrt{1 - 1/\Gamma^2}$. The time-scale on which this energy will be dissipated may be approximated to be the crossing-over time of the two blobs,

$$T_{ON,K} \approx \frac{2\Delta x_K}{c(\beta_{2K} - \beta_{1K})} \quad (4)$$

where, Δx_K is the average size of the two blobs in the rest frame of the knot. It is assumed that this dissipated bulk kinetic energy, ΔE_K , gets converted efficiently to the energy of the non-thermal particles produced during the collision. The number of non-thermal particles injected per unit time into the knot is taken to be,

$$Q_K(\gamma)d\gamma = A\gamma^{-p}d\gamma \quad \text{for } \gamma > \gamma_{min}; \quad (5)$$

where γ is the Lorentz factor of the electrons, p is the particle index and A is the normalization constant given by,

$$A = \frac{\Delta E_K}{T_{ON,K}} \frac{(p-2)}{mc^2} \gamma_{min}^{(p-2)} \quad (6)$$

Here the injection is assumed to be uniformly occurring for a time $T_{ON,K}$. The cloud is permeated with a tangled magnetic field B_K .

The kinetic equation describing the evolution of the total number of non-thermal particles in the system, $N(\gamma, t_K)$, is

$$\frac{\partial N_K(\gamma, t_K)}{\partial t_K} + \frac{\partial}{\partial \gamma} [P(\gamma, t_K)N_K(\gamma, t_K)] = Q_K(\gamma) \quad (7)$$

$P(\gamma, t)$ is the cooling rate given by

$$P(\gamma, t_K) = -(\dot{\gamma}_S(t_K) + \dot{\gamma}_{IC}(t_K)) \quad (8)$$

where $\dot{\gamma}_S(t_K)$ and $\dot{\gamma}_{IC}(t_K)$ are the cooling rates due to synchrotron and Inverse Compton of the CMBR respectively (Sahayanathan *et al.* 2003).

The non-thermal particle distribution $N_K(\gamma, t_K)$ produces the synchrotron and Inverse Compton spectra which are computed at an observation time $t_K = t_{K,O}$. The Inverse Compton spectrum is computed after taking into account the anisotropy of the CMBR spectrum in the rest frame of the plasma (Dermer 1995). Finally, the flux is transformed from the source frame to the observer's frame in earth taking care of the Doppler boosting (Begelman *et al.* 1984) and cosmological effects.

Eqn (7) can be solved analytically (Kirk *et al.* 1998) or numerically computed using the technique given in Chang & Cooper (1970). Rather than the complete analytical expression it is perhaps more illuminating to study the asymptotic limits. It is convenient to define a critical lorentz factor γ_c for which the cooling time-scale for synchrotron and IC losses is equal to the observation time $t_{K,O}$. Then for $\gamma \ll \gamma_c$, there is effectively no cooling and the particle spectrum is $N(\gamma, t) \propto \gamma^{-p}t_{K,O}$ i.e. the injection rate times the observed time. For $\gamma \gg \gamma_c$ the cooling time is shorter than the observed time and hence the particle spectrum is in quasi-equilibrium $N(\gamma, t) \propto \gamma^{(p-1)/2}$. These two regimes in the particle spectra give rise to a composite synchrotron spectra with a spectral break.

Adiabatic cooling has been neglected in Eqn (7). The adiabatic cooling time-scale, t_{adb} is $\approx R(t)/v_{exp}$ where $R(t)$ is the size of the knot and v_{exp} is the speed at which the blob is expanding. Since $R(t_{K,O}) = R_i + v_{exp}t_{K,O}$, where R_i is the initial size of the knot, it follows that t_{adb} is always greater than t_{obs} for the case when the initial size of the blob $R_i \approx R(t_{K,O})$ and hence adiabatic cooling can be neglected. In the other extreme, if $R_i \ll R(t_{K,O})$, t_{adb} is at most t_{obs} . For $\gamma \gg \gamma_c$, the cooling time-scale is much smaller than $t_{obs} \approx t_{adb}$ and hence adiabatic cooling may still be neglected. For $\gamma \ll \gamma_c$, since $t_{K,O} \approx t_{adb}$ and not much larger, the effect of adiabatic cooling can only change the number density by a factor of few. Thus for an order of magnitude calculation as required for this work, adiabatic cooling can always be neglected.

The predicted spectrum and size of a knot depends on nine parameters, which are the mass of the blobs M , their average size Δx_K , the Lorentz factors Γ_1 and Γ_2 , the particle injection index p , the minimum Lorentz factor γ_{min} , the initial magnetic field B_0 , the inclination angle of the jet θ and the observation time $t_{K,O}$.

From these parameters and the location of the knot in the sky plane, one can infer the time delay Δt_{12} between the ejection of the two blobs. The projected distance of the knot from the source S can be written as

$$S = c(\beta_{1t_c} + \beta_{t_O}) \sin\theta \quad (9)$$

where $t_O = \Gamma t_{K,O}$ is the time of the observation after the formation of the knot in the source frame. The time elapsed t_c , after the ejection of the first blob and the start of the collision, is given by,

$$t_c = \frac{v_2\Delta t_{12} - \Delta x_1}{v_2 - v_1} \quad (10)$$

where Δx_1 is the size of the first blob $\approx \Gamma_{1,K}\Delta x_K/\Gamma$. Thus Δt_{12} , can be estimated using the above equation where t_c is given by Eqn (9), and it essentially depends on four parameters, θ , Γ_1 , Γ_2 and $t_{K,O}$.

A total time t_{tot} can be defined to be the time that has elapsed between the ejection of the first blob and the observation, $t_{tot} = t_c + t_O$. For two knots, A and B, the time difference between the ejection of their first blobs, t^{AB} is then

$$t^{AB} = t_{tot}^A - t_{tot}^B - t_{LT} \quad (11)$$

where t_{LT} is the light travel time difference between the two knots which is approximated to be

$$t_{LT} = \frac{S^A - S^B}{c \tan\theta} \quad (12)$$

The power of the jet, can be defined in two different ways. The instantaneous power, which is the power when the system

is active, can be defined to be the average energy of the blobs divided by the time-scale on which the blobs are ejected. This power can be estimated for each knot to be

$$P_{ins} \approx \frac{Mc^2(\Gamma_1 + \Gamma_2)/2}{\Delta t_{12}} \quad (13)$$

On the other hand, the time averaged power of the jet can be defined as the typical energy ejected during active periods divided by the time-scale on which such activity occur. For two knots, A and B, this can be approximated to be

$$P_{ave} \approx \frac{[M^A c^2(\Gamma_1^A + \Gamma_2^A) + M^B c^2(\Gamma_1^B + \Gamma_2^B)]/2}{\Delta t^{AB}} \quad (14)$$

Two *a posteriori* checks have to be imposed to ensure self-consistency. The total number of non-thermal particles that is injected, N_{nth} should be less than the number of particles in the knot, $N_K \approx 2M/m_p$ and that the magnetic field $B_K(t_K)$ should be less than the equipartition value, B_{equ} .

4. RESULTS AND DISCUSSION

The model has been applied to those knots of kpc-scale jets, which have been detected by *Chandra*, and for which radio and optical data are available. This criterion was satisfied by the two brightest knots of the AGN: 1136–135, 1150+497, 1354+195, 3C273 and 3C371. In this work, the knot closer to the nucleus is referred to as Knot A and the further one as Knot B. For these sources this nomenclature is same as in the literature except for 3C371 where the farther one has been referred to as Knot A. For three of these sources, the X-ray spectral indices were constrained using long exposure observations as described in §2. The observed properties of the sources and the knots are tabulated in Table 1 and 2.

Figure 1 shows the observed radio, optical and X-ray fluxes of these knots, along with the computed spectra corresponding to model parameters that are given in Table 3. Since the number of parameters is large as compared to the observables, a unique set of parameter values cannot be obtained. Two consistency checks have been imposed on the parameter values, which are that the number of non-thermal electrons which will be injected into the system, N_{nth} , is smaller than the total number of protons, N_k , and that the magnetic field, B is less than the equipartition value, B_{equ} . Both these conditions are satisfied by the parameter sets as shown in Table 3, where the ratios B/B_{equ} and N_{nth}/N_K are given.

For each source, the time delay, Δt_{12} , between the ejection of the two blobs which form the knots are nearly equal to the time difference between the ejection of the first blobs of Knot A and Knot B, t^{AB} . This gives an overall *single* time-scale of activity for each source which ranges from $10^{11} - 10^{12}$ sec which can reproduce the knot properties as had been assumed in the development of the simple internal shock model. This result is important since if it had not been true a more complex temporal behavior would have to be proposed, wherein the jet structure is due to variability of the source in two different time-scales. The first being the time difference between the ejection of two blobs that form a knot and the second being the time difference between the activities that produced the two knots.

The cross over time, $T_{ON,K}$, is determined here by Eqn. 4. Since, $\beta_{2K} - \beta_{1K} \approx (\Gamma_1 - \Gamma_2)/\Gamma \approx 0.3$, $T_{ON,K} \approx 10^{12} (\Delta x_K / 5 \times 10^{21} \text{cm})$ sec. During this time, i.e. the time when there is injection of particles into the system, the knot would travel a distance $\approx cT_{ON} \approx c\Gamma T_{ON,K} \approx 50(\Gamma/5)(\Delta x_K / 5 \times 10^{21} \text{cm})$

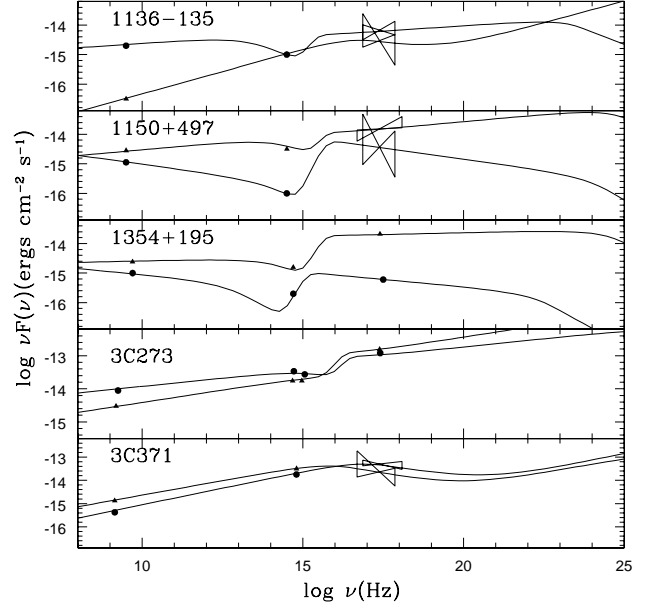


FIG. 1.— The observed fluxes in radio, optical and X-ray compared with model spectra using parameters given in Table 2. Knot A fluxes are represented by filled triangles and knot B fluxes are represented by filled circles. Errors are typically 30% or larger.

kpc. This is a significant fraction of the total observable distance traveled by the knot, from formation $\approx ct_c \approx 100$ kpc (see Table 3) to the termination of the jet in the radio lobe, ≈ 200 kpc. Hence, as shown in Table 4, it is possible to fit the spectra of all the knots, with an observation time, $t_{O,K}$ which is less than the crossing over time, $T_{ON,K}$ implying that there is continuous injection of particles into the system. In this scenario, the synchrotron and IC spectra have a break corresponding to a Lorentz factor, γ_c , where the cooling time-scale equals the observation time (Sahayanathan *et al.* 2003). This is in contrast to one-time injection models (i.e. when $t_{O,K} > T_{ON,K}$) where an exponential cutoff in the spectra occurs. However, this does not exclude the possibility that for some knots, $t_{O,K} > T_{ON,K}$ and such cutoff in spectra would be detected.

The knots of 3C371 and Knot A of 1136-135 are unique in this sample since their the X-ray flux lies below the extrapolation of the radio/optical spectra to X-ray wavelengths. This allows for the interpretation that the X-ray flux is due to synchrotron emission (Sambruna *et al.* 2002; Pesce *et al.* 2001; Sahayanathan *et al.* 2003). For Knot A of 1136-135 and Knot B of 3C371, this implies that the spectral break for the synchrotron emission occurs at the X-ray regime (Figure 1) which in turn indicates that these sources are relatively younger ones. Indeed, the ratio of the observation time to the time-scale of injection, $t_{O,K}/T_{ON,K}$ for these sources are smallest (Table 4). On the other hand, for Knot A of 3C371, the spectral break can occur at the optical band even if the X-ray flux is interpreted as being due to synchrotron emission (Figure 1) and hence this source need not be relatively young. However, this is only possible if $t_{O,K} < T_{ON,K}$ and there is continuous injection of particles. Otherwise, a sharp cutoff in the spectrum at the optical band would have occurred and the X-ray emission would not be due to synchrotron emission.

TABLE 3
MODEL PARAMETERS

Source	Knot	θ	Γ_1	Γ_2	Γ^*	t_{KO}	t_c^*	t_{tot}^*	log M	γ_{min}	p	B
1136–135	A	11.5	4.6	5.4	5.0	0.25	11.8	11.6	38.0	2	2.4	1.1
	B		4.1	5.9	5.0	8.5	13.1	17.3	36.4	20	2.9	4.5
1150+497	A	10.2	2.5	3.0	2.8	16.0	1.2	5.1	37.5	30	2.8	1.4
	B		2.6	3.5	3.0	6.2	8.8	10.0	36.8	30	3.3	4.0
1354+195	A	8.21	1.7	2.3	2.0	9.0	8.1	8.1	38.1	37	3.0	1.7
	B		1.7	2.3	2.0	8.7	15.0	17.0	37.1	20	3.2	8.0
3C273	A	8.23	2.2	4.0	3.1	2.1	27.0	24.0	36.8	50	2.7	0.4
	B		1.7	2.3	2.0	8.0	30.0	32.0	37.8	80	2.8	0.6
3C371	A	15.8	1.6	2.4	2.0	5.9	0.18	1.4	35.5	20	2.5	1.0
	B		2.0	2.4	2.2	2.3	0.39	0.75	36.8	10	2.4	0.6

NOTE. — Seven of the model parameters and derived quantities. The eight parameter, $\Delta x_K = 5.0 \times 10^{21}$ cm for all sources. Columns marked with * are derived quantities and not parameters. Columns:- 1: Source name. 2: Knot. 3: Viewing angle (in degrees). 4: Lorentz factor of the first blob. 5: Lorentz factor of the second blob. 6: Lorentz factor of the Knot. 7: Observation time (in 10^{11} sec). 8: Collision time (in 10^{12} sec). 9: Total time (in 10^{12} sec). 10: Mass of the blobs (in g). 11: Minimum Lorentz factor of the particle injected into the knot. 12: Injected particle spectral index. 13: Magnetic field (in 10^{-5} G).

TABLE 4
KNOT/JET PROPERTIES

Source	Knot	Δt_{12}	t^{AB}	$\frac{B}{B_{equ}}$	$\frac{N_{nth}}{N_K}$	log P_{ins}	log P_{ave}	$T_{ON,K}$	$\frac{t_{K,O}}{T_{ON,K}}$	D
1136–135	A	1.1	3.1	0.55	0.88	48.60	48.17	20.4	0.01	112.8
	B	2.5		0.74	0.74	46.65		9.1	0.93	163.4
1150+497	A	0.9	5.0	0.12	0.13	47.98	47.31	17.0	0.94	50.5
	B	3.9		0.65	0.43	46.63		10.7	0.58	96.1
1354+195	A	7.5	18.0	0.04	0.38	47.49	47.15	9.6	0.94	78.7
	B	17.0		0.64	0.78	46.10		9.6	0.90	135.5
3C273	A	20.0	34.0	0.03	0.80	46.00	46.63	5.4	0.39	240.7
	B	31.6		0.02	0.16	46.60		9.6	0.84	248.5
3C371	A	1.4	1.5	0.39	0.88	45.59	46.98	7.2	0.83	11.2
	B	1.0		0.28	0.29	47.14		16.3	0.14	7.7

NOTE. — Columns:- 1: Source name. 2: Knot. 3: Time delay between the ejection of the blobs (in 10^{11} sec). 4: Time delay between the ejection of the first and the third blob (in 10^{11} sec). 5: Ratio of the magnetic field to equipartition magnetic field. 6: Ratio of non-thermal electrons to the total number of electrons. 7: The instantaneous power (in ergs/sec). 8: Time averaged power (in ergs/sec). 9: Time-scale over which non-thermal particles are injected (in 10^{11} sec). 10: Ratio of the observation time to particle injection time-scale. 11: Deprojected distance in kilo parsec

Figure 1 shows that the radio, optical and X-ray spectral indices for different knots may vary and highlights the need for more spectral measurements in all bands. A definite prediction of this model is that for most knots, the X-ray spectral index should be equal to the radio one, indicating that the X-ray flux is due IC/CMBR. Such spectral constrains would be particularly important since, although it has been demonstrated here that the internal shock model can explain the broad band spectra of these sources, there could be other models which may be physically and observationally more favorable. Recently Jester *et al.* (2005) have analyzed VLA and HST image of 3C273 and have found that the optical and radio spectral indices are different indicating the presence of an additional emission mechanism for the source. Earlier, Atoyan & Dermer (2004) argued that the X-ray flux is due to a second population of non-thermal electrons, rather than being the IC/CMBR spectra of the same distribution which produces the radio and optical emission. They point out in the IC/CMBR model, since the X-ray emission is due to electrons which are only a factor ten more energetic than those which produce the radio, a source where the X-ray flux falls rapidly

from the center should also exhibit a similar decrease in radio emission which is not observed (e.g. 3C273 and 1354+195). Moreover, the jet power required in the IC/CMBR model can be very large $\approx 10^{48}$ ergs/sec, which may be larger than the power inferred from the giant radio lobes ($\lesssim 10^{47}$ ergs/sec). While the former argument may not strictly be applicable to the internal shock model (since each knot is a separate entity and the distance from the source is not a measure of the age of the source), the power requirement for some sources may indeed be very large, for e.g. Knot A of 1136-135 requires $P_{ave} \approx 2 \times 10^{48}$ ergs/sec (Table 3). However, the energy requirement may be decreased if the magnetic field is sub-equipartition e.g. 3C273 (Table 3). Thus it is desirable to obtain direct observational signatures, like spectral indices, to discriminate between models.

A realistic description of the knots will be more complicated than the simple model considered here. For example, the forward and reverse shocks that should form when the blobs collide, may provide different injection rates and at different locations within the Knot. However, the physics of these shock formations and the subsequent acceleration of

particles is complicated and unclear, especially if they are mediated by magnetic fields. In the future, results from sophisticated numerical simulations may be compared with higher resolution data (which can resolve the internal structure of the knots) to proof (or disproof) the internal shock model.

In summary, a simple internal shock model is consistent with the broad band spectra of knots in AGN kpc-scale jets. The age of the knots ($t_{O,k}$) may be smaller than the time-scale of injection of non-thermal particles ($T_{ON,K}$), which implies

there may be spectral breaks in the synchrotron and IC spectra, instead of exponential high energy cutoffs. The jets are powered by AGN, which sporadically eject out material on a 10^{11-12} sec time-scale.

The authors thank A. K. Kembhavi and C. L. Kaul for useful discussions.

REFERENCES

- Atoyan, A., and Dermer, C., 2004, ApJ, *in press* (astro-ph:0402647).
 Begelman, M. C., Blandford, R. D., Rees, M. J., 1984, Rev. Mod. Phys., 56, 255
 Biretta, J. A., Stern, C. P., and Harris, D. E., 1991, AJ, 101,1632
 Chang, J. S., and Cooper, G., 1970, Journal of Computational Physics, 6, 1
 Chartas, G. *et al.* , 2000, ApJ, 542, 655
 Dermer, C., 1995, ApJ, 446, L63
 Dermer, C., and Atoyan, A., 1995, ApJ, 568, L81
 Jaffe, W. J. & Perola, G. C., 1973, A&A, 26, 412
 Jester, S., Rosser, H-J, Meisenheimer, K. & Perley, R., 2005, A&A, 431, 477.
 Heavens, A., & Meisenheimer, K., 1987, MNRAS, 225, 335
 Kardashev, N. S., 1962, Soviet Astron.-AJ, 6, 317
 Kirk, J. G., Reiger, F. M., Mastichiadis, A., 1998,A&A, 333,452
 Lazzati, D., Ghisellini, G., & Celloti A.,1999, MNRAS, 309, L13
 Meisenheimer, K. *et al.* , 1989, A&A, 219, 63
 Marshall, H. L. *et al.* , 2001, ApJ, 549, 167
 Pacholczyk, A. G., 1970, Radio Astrophysics (San Fransisco : Freeman)
 Panaitescu, A., Spada, M., & Meszaros, P., 1999, ApJ, 522, L105
 Rees, M. J., 1978, MNRAS, 184, 61
 Rees, M. J., & Meszaros, P., 1994, ApJ, 430, L93
 Sahayanathan, S., Misra, R., Khembhavi, A. K., and Kaul, C. L., 2003, ApJ, 588, L77
 Sambruna. R. M. *et al.* , 2001, ApJ, 549, L161
 Sambruna, R. M. *et al.* , 2002, ApJ, 571, 206
 Schwartz, D. A. *et al.* , 2000, ApJ, 540, L69
 Spada, M., Ghisellini, G., Lazzati, D., and Celotti, A., 2001, MNRAS, 325, 1559
 Perlman, E. S. *et al.* , 2001, ApJ, 551, 206
 Pesce, J. E. *et al.* , 2001, ApJ, 556, L79
 Tavecchio, F., Maraschi, L., Sambruna, R. M., and Urry, C. M., 2000, ApJ, 544, L23
 Wilson, A. S., and Yang, Y., 2002, ApJ, 568, 133
 Worall, D. M., Birkinshaw, M., & Hardcastle, M. J., 2001, MNRAS, 326, L7